JOURNAL OF APPLIED ELECTROCHEMISTRY 20 (1990) 804–810

Structural modifications of a spent molten carbonate fuel cell

S. FRENI, N. GIORDANO

Istituto C.N.R.-T.A.E., Salita S. Lucia sopra Contesse, 39 - 98126 S. Lucia-Messina, Italy

S. CAVALLARO

Dipartimento di Chimica Industriale, Universitá di Messina, P.O. Box 29, 98010 Sant'Agata di Messina, Messina, Italy

Received 1 March 1989; revised 10 November 1989

Several performance and endurance tests have been carried out on molten carbonate fuel cells (MCFC) operating at different temperatures (873, 893 and 923 K). Electrochemical performance parameters, morphological characteristics and chemical analyses on samples of spent electrodes and tiles were evaluated. An output power decrease of 10% from the original value was taken to be the largest acceptable decay. Cell operation was stopped upon reaching this point. Electrolyte losses ranging from 18.6 to 24.5 of the original content were the determining factor in the MCFC performance decrease. Scanning electron microscopy showed that post-test anodes retained a satisfactory microstructure, while the tiles appeared to be very sensitive to the effect of operating temperature. The cathode structure, after an initial *in situ* oxidation, appeared to consist of agglomerates of 0.9 μm NiO crystallites. Long-term operation produces some modification of the pore size distributions of the used components, resulting in a final electrolyte distribution that was far from optimal. Due to the opposite effect of temperature on cell lifetime and power output, the highest power output and shortest cell lifetime were obtained for the 923 K test.

1. Introduction

The effect of temperature is paramount in determining the rates of the various processes that contribute to the performance and deterioration of a molten carbonate fuel cell (MCFC). Some researchers [1] have recently investigated the influence of temperature on parameters such as the electrolyte conductivity, the oxygen solubility, the cathodic and anodic exchange current densities, and the ionic diffusivity. On lowering the cell temperature from the base-line 923 K, the net effect was found to be, as expected, a decrease in the overall performance. In particular, between 923 and 873 K, the temperature effect on cell voltage appears to be moderate ($\approx 1.4\,mV\,K^{-1}$ at $I = 200\,mA\,cm^{-2}$) [1], while a larger decrease in the performance was recorded at the still lower temperature of 848 K ($2.2\,mV\,K^{-1}$ at $I = 200\,mA\,cm^{-2}$). On the other hand, upon raising the working temperature from 923 K, the useful life quickly decreases. Therefore the range 873–923 K is usually accepted as the optimal working temperature range, with preference for the base-line 923 K.

However, although much work has been carried out on the endurance of the MCFC [2–15], the mechanism of decay still needs to be evaluated case by case [3, 4]. In fact, whenever the electrochemical decay is not entirely attributable to macroscopic phenomena (such as anode creepage or gas crossover due to matrix fracture), it can be ascribed to some combination of several competing processes. NiO cathodes, for instance, slowly dissolve in the electrolyte; the Ni^{2+} ions migrate towards the anode and are reduced by H_2 to metallic Ni at some intermediate location between the two electrodes [5]. A fast cathode degradation is observed upon increasing the CO_2 partial pressure, so that a corresponding increase of the cathodic overpotential is obtained [6].

Anode sintering has also been suggested as another cause of decay [7]. To minimize this phenomenon, Cr (1–10 wt %) is added to the Ni plaques [8, 9], so that, by reaction with the electrolyte, a microporous surface layer of $LiCrO_2$ is created. Other researchers [10–12] have proposed covering the internal anode surfaces with a dispersed refractory oxide layer (Al_2O_3, $SrTiO_3$, $LiAlO_2$, etc.).

However, NiO cathodic corrosion or Ni anodic sintering cannot alone explain the performance decay under normal working conditions (low pressure of CO_2, life time < 10 000 h, etc.) and poor electrolyte management was identified as the main decay factor. In out-of-cell experiments, Ong and Claar [13] have been able to quantify the electrolyte losses due to vaporization. Based upon these results, with the only means of electrolyte loss via vapour transport in the anodic and cathodic streams, a typical cell should survive more than 15 000 h, which is contrary to the observations. Iacovangelo *et al.* [14] identified electrolyte creep, hardware corrosion and anode lithiation

0021-891X/90 $03.00 + .12

as the pivotal electrolyte consumption mechanisms while Donado *et al.* [15] emphasized that the severe electrochemical corrosion occurring in the wet seal area can be the main reason for the MCFC decay.

Since each of the above processes play an important role in the mechanism of decay, and temperature is known to influence them to different extents, optimizing the cell operating temperature might be a key factor in developing economical commercial power plants.

Following the above considerations, the present paper aims to reach a better understanding of the decay mechanisms of a conventional MCFC, with a final goal of optimizing the working temperature.

2. Experimental details

2.1. *Arrangement*

Endurance and performance tests on isothermal MCFCs were carried out in the completely automated monocell test-facility sketched in Fig. 1. The feeding pipelines were provided with appropriate manometers and rotameters in order to have a fine regulation of the gas flows. A pneumatic valve, installed on the fuel line, was controlled by leak detectors to assure safety conditions during the tests. Two temperature-controlled humidifiers were installed to give a preset water amount in each stream. Sampling points, before and after the cell, were provided to allow for gas-chromatographic analysis. Pressure and flow transducers to monitor data for mass and energy balances, a compressed air line for the holding piston and a water line to cool the condensers were also provided. The load simulation system consists of a DC power generator, which supplies a prefixed opposing current; the internal resistance (*IR*) of the cell was measured by the conventional current interruption technique (break time = 10^{-6} s). The data acquisition system (DAS) was a Hewlett-Packard 3487A data logger, supported by an HP 86 computer, and was able to manage from 20 to 1000 channels. In this way, the cell voltage and current, together with the transducer outputs, were also recorded by this DAS device.

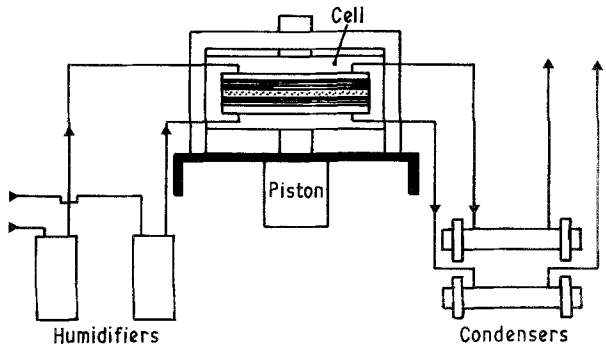

Fig. 1. Experimental apparatus.

To prevent any chemical or thermal shock from damaging the cell, the start-up and shut-down procedures were carefully programmed. Working conditions are detailed in Table 1.

2.2. *Analysis*

Chemical analyses for Li, K, Ni, Cr, Fe and Al, on the fresh and spent cell components were carried out using an atomic absorption (AA) Perkin Elmer model 4000 spectrophotometer. Porosimetric data were obtained by using a Carlo Erba Microstructure model 2000 Hg-intrusion porosimeter and scanning electron micrographs (SEM) were made by an Autoscan 'E TEC' 45A instrument coupled with a PV-9100 EDAX microprobe. The 'mean pore radius' (r_p) was evaluated as the numerical mean (Σ [$r \cdot$ %]). Following a common convention, porosity associated with $r < 0.1\ \mu$m was considered 'microporosity', with the remainder termed 'macroporosity'.

In order to quantify cross-over phenomena, gas chromatography analysis (GC) of gases entering and leaving the cell was made by two sampling valves in line, alternately connected to a Dani model 3800 gas-chromatograph with a 100–200 Carbosieve S-II, 10 ft × 1/8 in SS column. The temperature was programmed to remain for 7 min at 308 K, then to rise to 573 K at a rate of 32 K min^{-1}. The carrier gases were He for anodic streams or N_2 for cathodic streams with flow rates of 30–50 cm^3 min^{-1}. The thermal conductivity detector current was set at 150 mA.

Table 1. Synopsis of MCFC endurance tests.

Variables	*Units*	*Run 87/1*	*Run 85/4*	*Run 86/1*
Temperature	K	873	893	923
Pressure	Atm	1	1	1
Fuel flow	$cm^3\ min^{-1}$	255	255	255
Fuel comp.	%	60 H_2 + 40 CO_2	60 H_2 + 40 CO_2	60 H_2 + 40 CO_2
Fuel utiliz.	%	75	75	75
Oxidant flow	$cm^3\ min^{-1}$	915	915	915
Oxidant comp.	%	75 air + 25 CO_2	75 air + 25 CO_2	75 air + 25 CO_2
Oxidant utiliz.	%	44	44	44
In. power dens. (0.15 A cm^{-2})	mW cm^{-2}	102.1	114.9	118.1
Fin. power dens. (0.15 A cm^{-2})	mW cm^{-2}	91.9	103.4	106.3
Initial *IR*	mΩ	8	7.3	8
Final *IR*	mΩ	12	9	10
Life time	h	6400	4400	2200

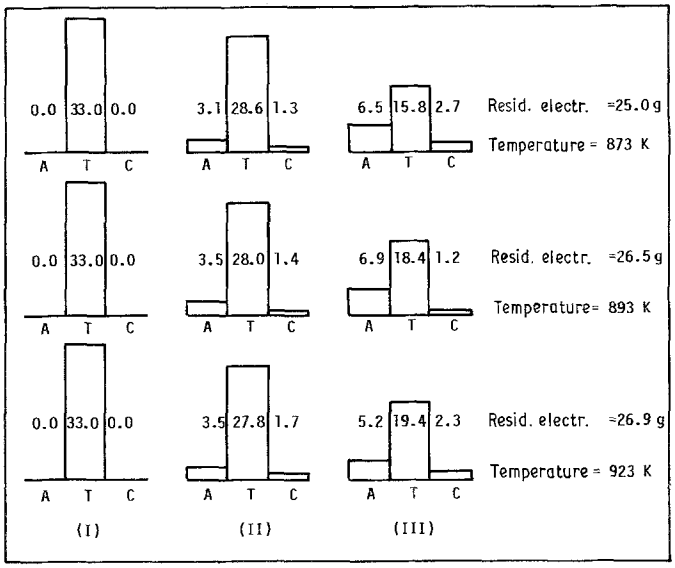

Fig. 2. Electrolyte distribution in MCFCs at 873, and 923 K: (I) initially; (II) 100 hr after the start; (III) post-mortem. A = anode; T = tile; C = cathode.

According to Maru *et al.* [16] the residual electrolyte in the post-test matrix (tile) was selectively dissolved by using a warm mixture of 50 wt % acetic acid/acetic anhydride; Al, K and Li mass balances were accounted for in separately derived AA analyses. The tile filling degree (tfd) was computed as the ratio of the volume of residual electrolyte in the tile to the final pore volume of the tile.

Anodes and cathodes were washed with cold water, to avoid Ni leaching, and chemical AA analysis of the wash solutions and of the solid electrode residuals were also performed.

The results of the porosimetric and SEM determinations, together with the chemical AA analyses, were compared for all components, so that a reasonable picture of the microstructure could be proposed for the entire spent cell.

2.3. *Materials*

The tested cell components were supplied by the Institute of Gas Technology (IGT) of Chicago (USA).

Fresh anodes, based on Ni with 10 wt % of Cr, were made by a tape-casting technique. Their thicknesses and weights ranged from 0.78 to 0.85 mm and 25.3 to 28.4 g, respectively. Prelithiated (Li 1 wt %) Ni cathodes, made by tape-casting, were oxidized *in situ* after assembling the cell. The thicknesses of the fresh cathodes ranged from 0.32 to 0.35 mm and their weights from 7.6 to 7.9 g. The $LiAlO_2$ tiles, charged with 55 wt % of the eutectic Li, K carbonate mixture, were made by the hot-pressing technique. Tile thicknesses ranged from 1.75 to 1.85 mm and their weights from 55.9 to 56.5 g. The useful area of the assembled cells was 94 cm^2.

The anodic current collector was made of a drilled Ni sheet, while the cathodic one was of AISI 316 to minimize its oxidation. Both current collectors were located in two AISI 316 housings, and two aluminum seals were interposed on the sealing area between the tile and the housings. In this configuration, the tile extending beyond the useful cell area acted as the wet seal.

3. Results

Table 2 summarizes the behaviour of the fundamental electrical variables during the test runs. First, irrespec-

Table 2. Initial and final measured values for test runs at temperatures of 873, 893 and 923 K

Test run	*Current (A)*	*Potential*		*Power density*		*Ohmic drop (IR)*	
		Initial (mV)	*Final (mV)*	*Initial ($mW\,cm^{-2}$)*	*Final ($mW\,cm^{-2}$)*	*Initial ($m\Omega$)*	*Final ($m\Omega$)*
86/1	0	1000	960	–	–	–	–
	5	950	860	48.4	45.7	8.0	10.0
	15	860	790	137.2	126.1	8.0	10.0
85/4	0	1015	1000	–	–	–	–
	5	930	880	49.5	46.8	7.3	9.0
	15	830	785	132.4	125.0	7.3	9.0
87/1	0	1020	995	–	–	–	–
	5	900	840	47.9	44.7	8.0	12.0
	15	760	575	121.3	91.0	8.0	12.0

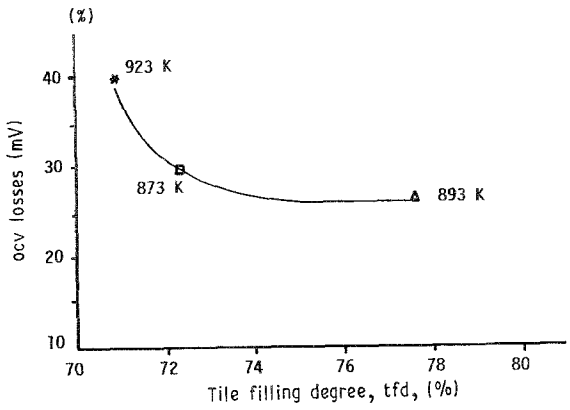

Fig. 3. Open circuit voltage (ocv) losses (mV) against the tile filling degree (tfd) (% of total porosity). Cell operating temperatures are shown, fuel comp. = 60% H_2 + 40% CO_2, oxid. comp. = 75% air + 25% CO_2, fuel flow = 255 $cm^3 min^{-1}$, oxid. flow = 915 $cm^3 min^{-1}$.

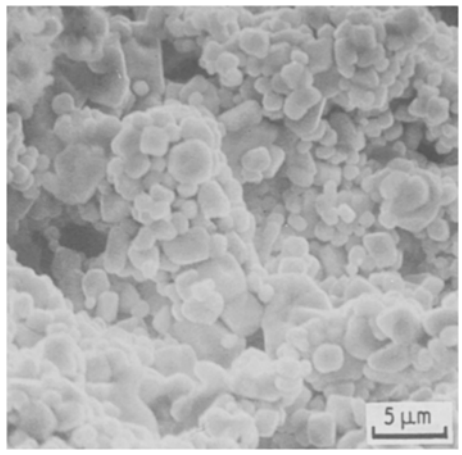

Fig. 4. SEM of the spent cathode.

tive of the cell temperature, the initial ohmic drop (*IR* values) were found to be close to 7–8 mΩ, with the final values ranging between 9 and 12 mΩ. The highest relative *IR* increase occurred at the lowest temperature. The output power appears to depend upon the working temperature. At the reference current density of 160 mA cm^{-2}, the initial power varied from 118.1 (923 K) to 102.0 (873 K) mW cm^{-2}, while the final power ranged from 103.7 to 91.0 mW cm^{-2}, respectively. As expected from the Nernst equation, the open circuit voltage (ocv) was found to vary inversely with the temperature from 1000 to 1020 mV. When the electrical power reached 90% of the initial value, each test was stopped, and the spent components were analyzed.

The amount and distribution of the residual electrolyte in each cell component is reported in Table 3. The measured total electrolyte losses seem to be correlated directly with the time and inversely with the temperature. In fact, the actual relationship between the electrolyte distribution and the time/temperature (t/T) variations is not immediately evident. A better overview of these aspects can be read from the histograms of Fig. 2. First, we observe that at the end of the useful lifetime, that is, when the power is 90% of its original value, the electrolyte losses are about 20 wt % of the initial content, a value which is only slightly dependent on the t/T variables. The percentage of total residual electrolyte found in the tile increases with the working temperature from 63.2 (873 K) to 72.1% (923 K), while the tile filling degree (tfd) does not seem to be related to the t/T variations. Otherwise, a clear relationship between the ocv drops and the tfd was found, as reported in Fig. 3.

The cathode microstructures, by SEM magnification at 3000–6000X, seem to be the same for all test runs. As shown in Fig. 4 for a typical cathode (run 86/1), the NiO-crystallite radius ranges from 0.3 to 2.3 μm with a mean radius of ~0.9 μm. The NiO agglomerate structure [17], is confirmed by porosimetric analysis which revealed both micro- (r_p = 0.1 μm) and macro-porosity (r_p = 5.0 μm) as related, respectively, to the pores between the adjacent NiO crystallites (filled by the electrolyte) and the large empty channels between the NiO agglomerates.

The SEM morphology of spent tiles is shown in

Table 3. Distribution and total losses of electrolyte measured after MCFC test run

	Electrolyte volume (cm^3)	*Porosimetric volume* (cm^3)	*tfd* (%)	*Electrolyte distribution* (%)	*Total electrolyte loss* (%)
Run 873 K					
Anode	2.94	4.572	64.3	26.0	
Cathode	1.22	2.520	48.2	10.0	24.5
Matrix	7.15	9.820	72.8	63.2	
Run 893 K					
Anode	3.17	3.719	85.2	26.2	
Cathode	0.56	2.190	25.6	4.6	19.4
Matrix	8.36	10.720	77.9	69.2	
Run 923 K					
Anode	2.34	4.400	53.0	19.2	
Cathode	1.07	2.670	40.0	8.7	18.6
Matrix	8.80	12.400	71.0	72.1	

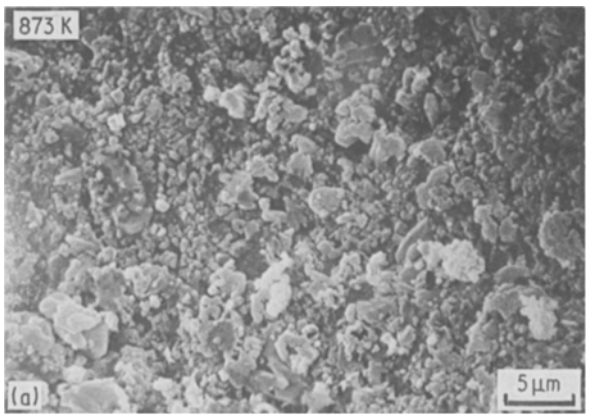

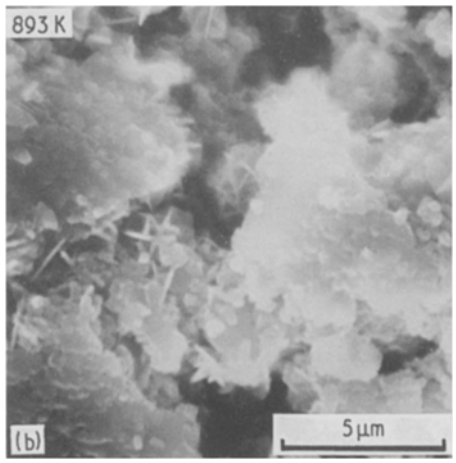

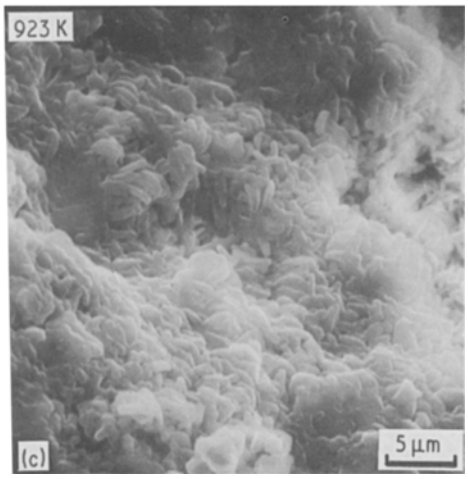

Fig. 5. Spent tile SEMs showing the morphological variations at (a) 873, (b) 893 and (c) 923 K.

Fig. 5. Figs 6 and 7 contain relative porosimetric data for the tiles. It is notable that the total porosity and the micropore volume fraction increase with the temperature and decreases with the cell life time. Moreover, the SEM micrographs show the presence of different $LiAlO_2$ forms depending upon the test conditions.

The phase distribution evaluation starts from the following structural observations [18]:

(1) The α-$LiAlO_2$ shows needle-like crystalline, roughened agglomerates with an average diameter of $\sim 5\,\mu m$. The measured distances between two agglomerates were in the range 3.0–8.0 μm, which justifies the existence of macro-pores with sizes of that same order of magnitude. The β-$LiAlO_2$ consists of typical 1–3 μm long rod-shaped crystals. Some bipyramidal crystals (0.5 μm × 2.0 μm) found could be attributed to the γ-$LiAlO_2$ phase.

(2) As shown in Fig. 5, although all $LiAlO_2$ phases were present together in each tested sample, only negligible traces of γ-phase were always detected. The low-T sample (873 K) showed a high percentage of the α-phase, whilst at the intermediate temperature, the β-phase was slightly predominant.

(3) No noticeable differences were detected among all spent anodes. A typical structure is shown in Fig. 8. The Ni/Cr (10%) anodes exhibited a framework of smooth cylindrical branches with diameters

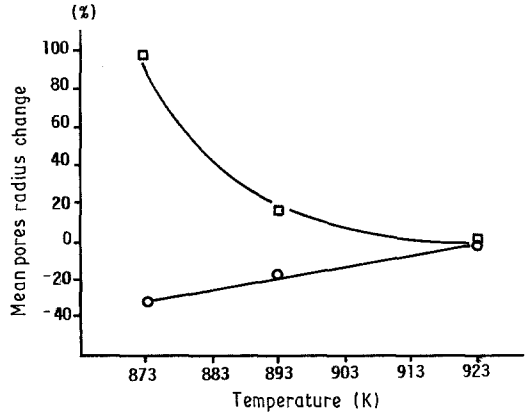

Fig. 6. Spent tile porosity variation (%) against operating temperature. The porosity variation is defined as $(\phi^\circ - \phi^f)/\phi^\circ$, where '$\phi^\circ$' and '$\phi^f$' are the initial and final porosities respectively, (□) micropores ($< 0.1\,\mu m$), (○) macropores ($> 0.1\,\mu m$).

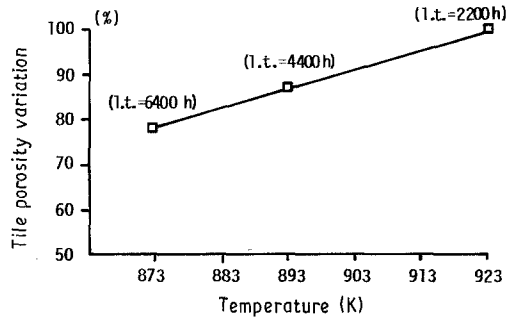

Fig. 7. Spent tile mean pore size variation (%) against operating temperature. The mean pore size variation is defined as $(r_p^f - r_p^0)/r_p^0$, where 'o' and 'f' denote initial and final values. Fuel comp.: 60% H_2 + 40% CO_2; oxid. comp.: 75% air + 25% CO_2; fuel flow: 255 $cm^3\,min^{-1}$; oxid. flow: 915 $cm^3\,min^{-1}$.

of 1–2 μm, spotted by $\sim 0.5\,\mu$m nodules, which were attributed to $LiCrO_2$ formation. The density of nodules on the surface was found to decrease linearly with temperature. Anode macroporosity, due to the empty space between the branches, ranged from 30 to 70% of the total pore volume ($\sim 150\,mm^3\,g^{-1}$) with a mean macropore radius of $r_p \sim 5\,\mu$m.

4. Discussion

The spent cathode is very different from the prelithiated (Li = 1 wt %) Ni electrode used as the starting material. High temperature oxidation, in fact, modifies the initial smooth structure, turning it into agglomerates of NiO crystallites (Fig. 4). The electrolyte filled micropores between the crystallites provide some structural stability under normal working conditions. By washing the spent cathode under progressively stronger conditions (cold water → warm water → acetic acid), the electrode gradually becomes an incoherent black powder, and the washing solution is enriched in Li and K and in Ni, which slowly dissolves in an acidic medium.

The structure of the spent cathodes appeared weakly sensitive to the effect of the t/T variations, showing no appreciable differences amongst the different samples as to total porosity and pore size distribution. Some decrease of the micropore radius was found in going from low to high temperature and is probably due to the different oxidation level reached at each working temperature. The most evident cathode decay process can be associated with the non-negligible NiO solubility in the carbonate mixture [6]. NiO dissolves through either acidic or basic mechanism, following the reactions [19]:

$$NiO + CO_2 \longrightarrow Ni^{2+} + CO^{2-} \qquad (1)$$

and

$$NiO + \tfrac{1}{2}Li_2CO_3 + \tfrac{1}{4}O_2 \longrightarrow NiO_2^- + \tfrac{1}{2}CO_2 + Li^+ \qquad (2)$$

These mechanisms are strictly correlated to the acidity degree of the carbonates mixture. For an MCFC, working at standard conditions, cathode dissolution through an acidic mechanism has been postulated and proven [6], its rate being favoured by an increase in the CO_2 partial pressure. According to Baumgartner [6], Ni^{2+} dissolves at the cathode and slowly diffuses towards the anode where, due to the anodic H_2 chemical reductant action, the Ni^{2+} precipitates as metallic Ni which is easily monitored in the white spent tile as a black front line. However, for an MCFC working at atmospheric pressure, cathode dissolution does not appear to be a determining cause of decay, at least for tests running less than 10 000 h [6, 20].

As represented in Fig. 8, no significant modifications have been observed for the anode. Only $LiCrO_2$ nodules, spread over the smooth Ni branches, reveal some electrode modification with respect to the initial anodic structure [7]. Micropores created by the interparticle free-spaces (Table 3), comprise 50–85% of the total anode porosity and account for the good wettability of the anode as shown in Fig. 2. The total pore volumes and pore size distributions of the spent anode samples were all found to be very similar, showing a reproducible manufacturing technique. Slight differences in the microporosity were observed between the used and fresh anodes. This is attributable to the different degrees of lithiation produced by the t/T variation. From a chemical point of view, the anodic composition appears to be stable, too.

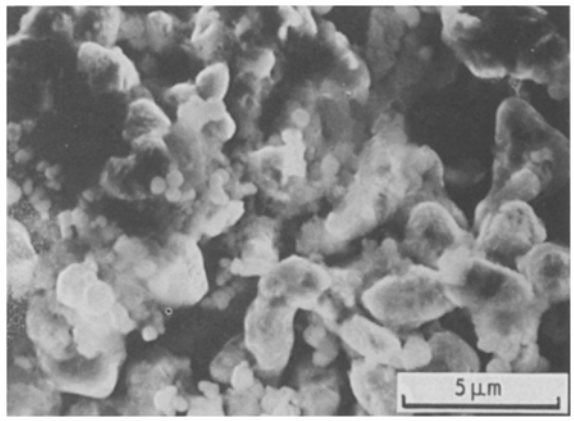

Fig. 8. SEM of the spent anode.

The only chemical difference observed is for the Cr content which shows small increases with respect to the fresh anode. This is probably due to the corrosion of the cell housings.

By contrast structural and chemical modifications were very evident in the used tiles. In fact, as revealed in Figs 2, 5, 6 and 7, the electrolyte amount and the $LiAlO_2$ phase distributions vary greatly by virtue of the t/T variations. The combined t/T effects caused the original α,β-$LiAlO_2$ structure to be slowly transformed into the more thermodynamically stable γ phase. This was not the only observed effect, as the tile structure was also found to be sensitive to the t/T variation. As reported in Fig. 7, an appreciable increase of the micropore radius was found in the longer life (lower temperature) tested samples. This modification in the tile structure caused a decrease in the electrolytic capacity of the tiles, and also a corresponding change in the electrolytic partitioning among the electrodes and the tile (see Fig. 2). As a result of these changes an appreciable number of empty pores were created permitting H_2 diffusion to occur. The effect of this large amount of reducing gas in the tile is an increase of the H_2 partial pressure on the cathode side (cross-over phenomenon) with a consequent drop in ocv of 30–40 mV, measured at the end of the tests [20]. In the highest temperature test, the original amount of electrolyte in the tile was kept to a maximum, demonstrating a good tile capability. Instead, in the lowest temperature test, the residual tile content was low, too high in the cathode, and only the anode was satisfactorily filled. We also noticed that the observed losses of electrolyte are in agreement

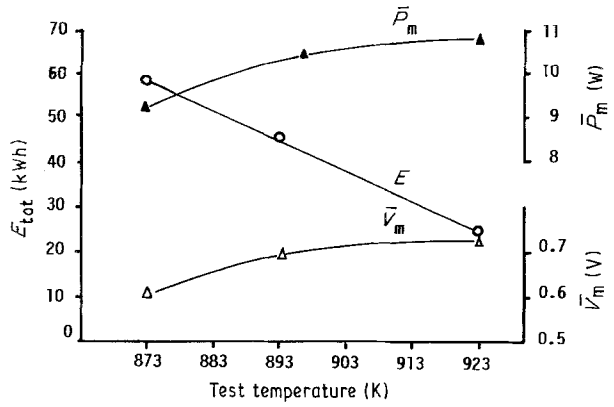

Fig. 9. Total energy (○), average voltage (△) and average electrical power (▲) against test temperature.

with values calculated from the empirical law proposed by Marianowski [21]. It seems that keeping electrolyte losses below 20% is crucial for the life of an MCFC, independent of the running time.

To conclude, we note some interesting conclusions about the magnitude of the energy and power released over the different lifetimes of each test run. For each test run, the total energy released (E_{tot}), the average power ($\bar{P}_m$) and the average voltage ($\bar{V}_m$) have been calculated from the equations

$$E_{tot} = I \int V \, dt$$

$$\bar{V}_m = \frac{\bar{E}_{tot}}{It}$$

$$\bar{P}_m = I\bar{V}_m$$

where all calculations are referred to a current of 15 A. Fig. 9 shows a cumulative plot of E_{tot}, $\bar{V}_m$ and $\bar{P}_m$ against the working temperature. It may be noted that the released energy increases with decreasing temperature, while $\bar{V}_m$ and $\bar{P}_m$ show an opposite trend.

5. Conclusions

Our performance and endurance tests on MCFC indicate that electrolyte management is one of the most critical factors affecting the life of the cells. Within a temperature range of only 50 K, a remarkable difference in the lifetimes was found: 2200 h at the highest temperature and 6400 h at the lowest temperature. Another meaningful aspect is related to the relatively low difference in the residual electrolyte content. In fact, independent of test conditions, the output power drops off until the 90% of the starting value when the electrolyte losses reach 20–25 wt % of the original charge (33.0 g). Post-mortem analysis revealed that electrolytic partition among the cell elements (tile-electrodes) was very similar for each test temperature: anode = 19.2–26.2%; tile = 71.0–77.9%; cathode = 4.6–10.0%. Porosimetry and SEM micrography on the spent cells demonstrated that the anode structure was well-maintained, while significant $LiAlO_2$ phase transformation has been observed for the tiles employed at different temperatures. The cathodic NiO-agglomerate structure is produced by the action of oxidant stream on the fresh, prelithiated Ni cathode. The cathode appears to be slowly dissolving under the action of CO_2. The released energy linearly decreases against the MCFC temperature, while the output power shows an inverse behaviour. This allows us to conclude that if the MCFC system is optimized to provide the cheapest energy production, it seems more advantageous to work at lower temperature, while if a high power is required, the system benefits from the highest temperature (923 K).

Acknowledgement

Part of this work has been carried out under contract of European Community (Non Nuclear Energy Program contr. # EN 3E-0086-I). SEM analysis was carried out at CNR-IRTEC (Faenza, Italy).

References

[1] Energy Research Corporation (ERC), *Final Report*, GRI 5081-244-0545 (1983).
[2] N. Giordano, S. Freni, R. Quagliata, S. Cavallaro and P. Carbonaro, *J. Electrochem. Soc.* **135** (1988) 910.
[3] K. Otsuka, T. Kahara and R. Oshima, Proc. 'Fuel Cell Technology and Applications', Seminar, Holland (1987) 51.
[4] N. Giordano, S. Freni, S. Cavallaro and P. Carbonaro, *Int. J. of Hydrogen En.* **14** (1989) 339.
[5] R. D. Pierce, J. L. Smith and R. B. Poeppel, in 'Molten Carbonate Fuel Cell Technology' (edited by J. R. Selman and T. D. Claar). The Electrochemical Society, Pennington, NJ (1984) p. 147.
[6] C. E. Baumgartner, *J. Am. Ceramic Soc.* **69** (1986) 162.
[7] C. D. Iacovangelo, *J. Electrochem. Soc.* **133** (1986) 2410.
[8] Energy Research Corporation (ERC), *Final Report*, DOE-ET-11304-19 (1980).
[9] Institute of Gas Technology (IGT), Contr. EC-78-C-03-1735-3 (1978).
[10] D. L. Johnson, *EPRI EM-624 Project 371-1* (March, 1978).
[11] E. M. Perry, Masters' Thesis, Northwestern University, IL, USA (1982).
[12] Energy Research Corporation (ERC), *Final Report*, DOE-ET-11304-29 (1983).
[13] E. T. Ong and T. D. Claar, in 'Molten Carbonate Fuel Cell Technology' (edited by J. R. Selman and T. D. Claar). The Electrochemical Society, Pennington, NJ (1984) p. 54.
[14] C. D. Iacovangelo and E. C. Jerabek, *J. Electrochem. Soc.* **133** (1986) 280.
[15] R. A. Donado, L. G. Marianowski, H. C. Maru and J. R. Selman, *J. Electrochem. Soc.* **131** (1984) 2535.
[16] A. Pigeaud, G. Wilemski, D. Rigos and R. Chamberlin, Proc. 'Fuel Cell Seminar' (1986) 211.
[17] Physicsl Sciences Inc. (PSI), *Final Report*, Contr. DE-AC05-79ET-15403 (1982).
[18] J. R. Selman and H. C. Maru, 'Advances in Molten Salt Chemistry', vol. 4 (edited by G. Mamantov and J. Bramstein), Plenum Press, New York (1981).
[19] D. A. Shores, C. D. Iacovangelo and R. H. Wilson, Proc. '162nd Electrochem. Soc. Meeting', Detroit (1982).
[20] S. Freni, P. Carbonaro and V. Alderucci, *Int. Rep. 03/1988*, IST. CNR-TAE, Messina, Italy (1988).
[21] L. G. Marionowski and J. B. O'Sullivan, Proc. '8th Annual Energy Technol. Conf. and Exp.', Washington, DC (1981).